

## Searching for Black Hole Candidates in Quiescence by Using Multi-band Observations in Globular Cluster M22 (NGC6656)

YU-JING XU (徐雨婧) <sup>1</sup>, WEI-MIN GU (顾为民) <sup>1</sup>, XIN-YU FANG (方欣雨) <sup>1</sup>, SHAN-SHAN WENG (翁山杉) <sup>2</sup>, AND  
TAO AN (安涛) <sup>3</sup>

<sup>1</sup>*Department of Astronomy, Xiamen University, Xiamen, Fujian 361005, People's Republic of China*

<sup>2</sup>*School of Physics and Technology, Nanjing Normal University, Nanjing, Jiangsu 210023, People's Republic of China*

<sup>3</sup>*Shanghai Astronomical Observatory, 80 Nandan Road, 200030 Shanghai, People's Republic of China*

### ABSTRACT

We present a multi-wavelength investigation of radio sources in the globular cluster M22 (NGC6656) using *VLA*, *HST*, and *Chandra* observations. Among the eight identified counterparts, we highlight VLA22 as the most promising stellar-mass black hole (BH) candidate. Its radio and X-ray luminosities follow the established  $L_R - L_X$  correlation for quiescent black hole low-mass X-ray binaries (BH-LMXBs), while its moderately steep radio spectrum and X-ray spectral hardening further support this classification. Analysis of two potential optical counterparts—a bright main-sequence star and a faint subgiant/red giant—suggests a binary system with a relatively long orbital period. The discovery of VLA22 consistent with recent retention models that stellar-mass BH can be retained within globular clusters over Hubble timescales. Additionally, VLA19 exhibits a characteristically inverted radio spectrum ( $\alpha = 0.79 \pm 0.39$ ,  $S_\nu \propto \nu^\alpha$ ) indicative of a compact jet, while VLA40 also aligns with the BH  $L_R - L_X$  track, though both require further observations to definitively confirm their nature.

*Keywords:* stars: black holes - globular clusters: general - globular clusters: individual (M22) - X-ray: binaries

### 1. INTRODUCTION

Globular clusters (GCs) are remarkably efficient "factories" for exotic stellar systems. Despite accounting for only  $\sim 0.1\%$  of the Galactic stellar mass, they host approximately 10% of the low-mass X-ray binary (LMXB) population (Clark 1975). Old GCs are thought to have formed through the rapid, high-efficiency fragmentation of massive, high-pressure protogalactic gas clouds during the early stages of galaxy formation, leading to the creation of exceptionally dense and gravitationally bound stellar systems that have survived for over 12 billion years (Brodie & Strader 2006; Krumholz et al. 2019). As a part of old stars reach the late stages of their evolution, those with sufficient initial mass undergo gravitational collapse to form various types of compact objects, such as white dwarfs (WDs), neutron stars (NSs) and black

holes (BHs) (Heger et al. 2003). Historically, theoretical models suggested that stellar-mass BHs should be efficiently ejected from GCs. Driven by mass segregation, BHs would sink to the cluster center and undergo energetic three-body interactions which would impart large recoil velocities, leaving at most one or no BHs by the present day (Kulkarni et al. 1993; Sigurdsson & Hernquist 1993). However, this paradigm has been challenged by the detection of super-Eddington sources in extragalactic GCs (Irwin et al. 2010) and modern  $N$ -body simulations, which suggest that a significant BH population can survive and remain dynamically active over Hubble timescales (Sippel & Hurley 2013; Morscher et al. 2013).

Identifying BH candidates in GCs is challenging because most reside in a quiescent state with low accretion rates, making them difficult to distinguish from NS-LMXBs using X-ray data alone. Luckily, the commissioning and widespread application of high-sensitivity radio interferometers, most notably the Karl G. Jansky Very Large Array (*VLA*) and the Australia Tele-

scope Compact Array (*ATCA*), have enhanced our capability to study BH-LMXBs. BHs in quiescence or hard state are characterized by a flat-to-inverted radio spectrum ( $\alpha \gtrsim 0$ ;  $S \propto \nu^\alpha$ ) and follow a distinct  $L_X - L_R$  correlation, exhibiting higher radio luminosities than NS-LMXBs at comparable X-ray levels (Gallo et al. 2014a). Other radio sources, such as millisecond pulsars (MSPs), typically show steeper radio spectra ( $\alpha \approx -1.6$ ; Jankowski et al. 2018), while cataclysmic variables (CVs) and active binaries (ABs) generally remain below detection limits at GC distances (Drake et al. 1989; Abada-Simon et al. 1993; Osten et al. 2000; Marsh et al. 2016; Russell et al. 2016). Thus many systematic studies utilizing the  $L_X - L_R$  correlation and radio parameters to search for BH-LMXB candidates in GCs, such as M22, M62, M10 and 47 Tuc (Strader et al. 2012; Chomiuk et al. 2013; Miller-Jones et al. 2015; Shishkovsky et al. 2018).

M22 (NGC 6656), located at  $\sim 3.2$  kpc, is a prime target for such studies. The optical extinction is typically reported as  $E(B - V) \approx 0.34$ . In terms of its structural dimensions, M22 has a core radius ( $r_c$ ) of approximately  $1.42'$  and a half-mass radius ( $r_h$ ) of about  $3.26'$  (Harris 1996). Previous multi-wavelength surveys at X-ray and optical bands identified numerous low-luminosity X-ray sources, including confirmed CVs (Webb et al. 2004; Webb & Servillat 2013). Notably, Strader et al. (2012) identified two BH-LMXB candidates in M22 based on their flat radio spectra. However, these sources lacked X-ray counterparts, leaving their accretion physics poorly constrained. Since X-ray and optical data are essential for characterizing the accretion disk and companion star, a multi-frequency approach is required for robust identification.

In this work, we conduct a systematic investigation of M22 using *VLA*, *Chandra*, and *HST* observations, aiming to refine the classification of compact binaries in the cluster. Section 2 describes the data reduction and spatial matching; Section 3 presents the observational results and proposes a new BH-LMXB candidate; and Section 4 discusses the implications of our findings.

## 2. DATA ACCESS AND PROCESSING

### 2.1. Radio observations

The radio data utilized in this study originate from the Milky Way *ATCA* and *VLA* Exploration of Radio sources In Clusters (MAVERIC) survey. This survey targeted 61 Galactic GCs using the *VLA* and *ATCA*, leveraging their high sensitivity and sub-arcsecond spatial resolution to identify compact sources (Shishkovsky et al. 2020; Tudor et al. 2022). For the 25 GCs observed by the *VLA*, the data were flagged and cali-

brated using the Common Astronomy Software Application (CASA) and the Astronomical Image Processing System (AIPS) (Greisen 2003; McMullin et al. 2007). Sources were extracted using the AEGEAN algorithm with a significance threshold of  $> 5\sigma$ , and the resulting catalogs—containing flux densities at 5.0 and 6.8 GHz and radio spectral indices—were published via the VizieR platform<sup>1</sup>.

M22 was observed by the *VLA* in the B/BnA configuration during May 2011 (Project Code: 10C-109) with a total integration time of 10 h (7.3 h on-source). These observations utilized the C-band (4–8 GHz) with two 2 GHz bandwidths centered at 5.0 and 6.8 GHz. The synthesized beam sizes achieved were  $1.54'' \times 0.81''$  and  $1.14'' \times 0.59''$ , with corresponding RMS noise levels of 2.4 and  $2.0 \mu\text{Jy}/\text{beam}$ , respectively. Within M22, 47 radio sources were detected, including 13 within the core radius ( $r_c$ ) and 6 outside the half-light radius ( $r_h$ ). We adopted this catalog for our analysis, maintaining the original source numbering based on flux density. Positional uncertainties were determined by taking the maximum of the cataloged errors and a systematic error of approximately 10% of the beam size (Shishkovsky et al. 2020), typically resulting in a final uncertainty of  $0.15'' \times 0.1''$ .

### 2.2. X-ray counterpart searching

We utilized archival *Chandra* observations of M22 obtained in 2005 (16 ks; ObsID: 14609) and 2014 (86 ks; ObsID: 5437) using the Advanced CCD Imaging Spectrometer (ACIS). While Bahramian et al. (2020) provided a high-precision catalog (GCcat) for 38 GCs, we cross-referenced these results with the *Chandra* Source Catalog Release 2.0 (CSC 2.0, Evans et al. 2010). Due to its superior astrometric calibration against the Gaia DR3 reference frame, we adopted CSC 2.0 positions for spatial matching, while X-ray luminosities at 1–10 keV were derived from GCcat. We extracted all X-ray sources within a  $5'$  radius centered on M22. Positional uncertainties were conservatively defined as the maximum of the  $2\sigma$  cataloged error and a typical on-axis value<sup>2</sup> of  $0.5''$  (Garmire et al. 2003).

Initial cross-matching between the *VLA* and *Chandra* catalogs was performed using the Python package *Astropy*, yielding 8 counterparts listed in Table 1. For detailed spectral analysis, raw data were reprocessed us-

<sup>1</sup> <https://vizier.cds.unistra.fr/viz-bin/VizieR?source=J/ApJ/903/73>

<sup>2</sup> <https://cxc.harvard.edu/csc2/about.html>

**Table 1.** Radio–X-ray cross-matched sources in M22

VLA	$\alpha_{\text{VLA}}$ (h:m:s)	$\delta_{\text{VLA}}$ (d:m:s)	$S_{5\text{ GHz}}$ ( $\mu\text{Jy}$ )	$S_{7\text{ GHz}}$ ( $\mu\text{Jy}$ )	$r$ (arcmin)	loc.	$\alpha$	2CXO	$F_{1-10\text{ keV}}$ ( $\text{erg cm}^{-2}\text{ s}^{-1}$ )	$\Delta\text{pos}$ (arcsec)
10	18:36:36.471	−23:55:01.07	$52.5 \pm 2.8$	$40.4 \pm 3.6$	2.96	$r_{\text{h}}$	$-0.87 \pm 0.35$	J183636.4–235501	$6.11 \times 10^{-15}$	0.34
19	18:36:32.551	−23:55:28.63	$26.0 \pm 2.6$	$33.3 \pm 2.5$	2.3	$r_{\text{h}}$	$0.79 \pm 0.39$	J183632.5–235528	$9.57 \times 10^{-16}$	0.33
22	18:36:24.859	−23:55:14.95	$25.0 \pm 2.7$	$19.5 \pm 2.1$	0.99	$r_{\text{c}}$	$-0.81 \pm 0.51$	J183624.8–235514	$6.62 \times 10^{-14}$	0.15
25	18:36:09.529	−23:53:21.18	$24.1 \pm 3.4$	$14.6 \pm 3.9$	3.42		$-1.69 \pm 0.97$	J183609.5–235320	$1.66 \times 10^{-15}$	0.69
28	18:36:31.471	−23:52:54.68	$23.3 \pm 2.5$	$16.2 \pm 2.6$	2.2	$r_{\text{h}}$	$-1.23 \pm 0.67$	J183631.5–235254	$7.45 \times 10^{-16}$	0.41
34	18:36:25.447	−23:54:51.74	$17.5 \pm 2.8$	$11.9 \pm 2.0$	0.67	$r_{\text{c}}$	$-1.27 \pm 0.80$	J183625.4–235451	$1.28 \times 10^{-15}$	0.04
36	18:36:23.400	−23:55:20.15	$16.4 \pm 2.6$	$8.7 \pm 2.2$	1.06	$r_{\text{c}}$	$-2.03 \pm 0.85$	J183623.3–235520	$1.44 \times 10^{-15}$	0.42
40	18:36:20.486	−23:53:37.10	$14.7 \pm 2.6$	$<6.4 \pm 2.4$	1.03	$r_{\text{c}}$	$<0.4$	J183620.4–235336	$3.36 \times 10^{-14}$	0.56

NOTE— $r$  and loc denote the projected distance from the cluster center and the location relative to the core radius ( $r_{\text{c}}$ ) and half-light radius ( $r_{\text{h}}$ ) as reported in the radio catalog.  $\Delta\text{pos}$  is the radio–X-ray positional offset.

ing the *Chandra* Interactive Analysis of Observations<sup>3</sup> (CIAO) software (Fruscione et al. 2006, CALBD: 4.17) via the `chandra_repro` script. Spectra were extracted using `specextract`, and subsequent modeling was conducted in `XSPEC` (v12.15.0) (Arnaud 1996).

### 2.3. Hubble optical observations

The *HST* UV Globular Cluster Survey (HUGS; Piotto et al. 2015; Nardiello et al. 2018) provides a high-precision photometric baseline for M22, utilizing *HST*/WFC3 in F275W ( $UV_{275}$ ), F336W ( $U_{336}$ ), and F438W ( $B_{438}$ ), as well as *HST*/ACS in F606W ( $V_{606}$ ) and F814W ( $I_{814}$ ). We adopted HUGS as our primary dataset for Color-Magnitude Diagram (CMD) construction, and further integrated the WFPC2/F656N ( $H_{\alpha}$ ) narrow-band data (Obs ID: 5344) into our CMDs to facilitate the study of  $H_{\alpha}$  emission/absorption features. To investigate variability, we integrated 62 epochs of archival *HST*/WFPC2  $I_{814}$  data from 1999 (ObsID: 7615). Despite the two-decade gap, photometric consistency was verified using non-variable stars. Data were retrieved from MAST<sup>4</sup>, and PSF photometry was performed using `DOLPHOT` (Dolphin 2016), retaining only fits with  $\chi^2 < 5$ . Magnitude values are reported without extinction correction unless specified.

Astrometric matching was prioritized using ACS images, as its PSF sharpness and lower scattered-light levels provide superior resolution in dense environments (Sirianni et al. 2005). Furthermore, the ACS solution is precisely anchored to the Gaia frame, whereas WFC3 and WFPC2 images exhibit slight frame drifts.

Consequently, we first identified optical counterparts in the ACS frames before extracting multi-band photometry. We note that several faint counterparts detected in ACS remain below the detection threshold in the older WFPC2 data, precluding variability analysis for those specific targets.

Among the 8 identified X-ray/radio counterparts, six (VLA19, VLA22, VLA28, VLA34, VLA36, and VLA40) lie within the *HST* field of view. Their radio and X-ray positions, including uncertainty ellipses, are overlaid on the *HST*/ACS imaging in Figure 1.

## 3. RESULTS

### 3.1. M22-VLA22: The Most Promising Quiescent Stellar-Mass Black Hole Candidate

M22-VLA22 was detected at both 5 GHz and 7 GHz with a significance exceeding  $5\sigma$ . Located within the cluster core, it exhibits a radio spectral index of  $\alpha = -0.81 \pm 0.51$ . While the nominal value suggests a moderately steep spectrum, the large uncertainty remains consistent with the flat-to-inverted spectra ( $\alpha \gtrsim 0$ ) typically observed in quiescent BH-LMXBs. Assuming a flat spectrum at the cluster distance of 3.2 kpc, we derive a 5 GHz radio luminosity of  $L_{\text{R}} \approx 1.53 \times 10^{27}$  erg s<sup>−1</sup> ( $L_{\text{R}} = 4\pi d^2 \nu S_{\nu}$ , where  $\nu$  is the observing frequency). As shown in Figure 1, VLA22 is spatially coincident with the X-ray source 2CXO J183624.8–235514, with an offset of only 0.15″, well within the  $2\sigma$  X-ray error ellipse. The GCcat reports a 1–10 keV X-ray luminosity of  $L_{\text{X}} = 7.20 \times 10^{31}$  erg s<sup>−1</sup>. In the  $L_{\text{R}} - L_{\text{X}}$  plane (Figure 2), VLA22 is well consistent with the correlation line constructed by known quiescent stellar-mass BHs and exceeds the radio luminosities typical of CVs. A systematic analysis of 35 CVs by Ridder et al. (2023)

<sup>3</sup> <http://cxc.harvard.edu/ciao/>

<sup>4</sup> <https://mast.stsci.edu/search/ui/#/hst>

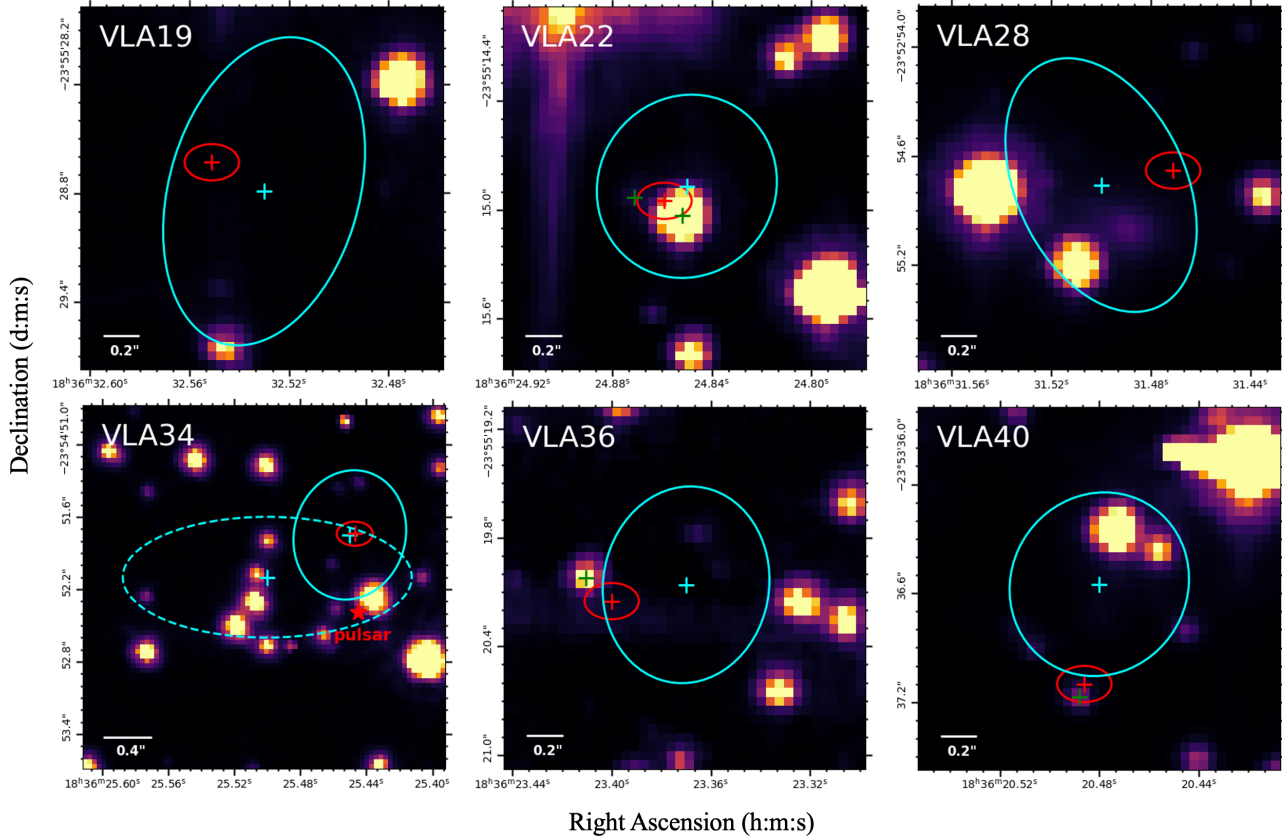


**Figure 1.** Multi-band identification map of six sources observed in all radio, optical and X-ray bands. The color background map shows the corresponding optical/infrared background from *HST*. The cyan cross and ellipse indicate the position and 95% error range of the coordinate given by *Chandra*, while the small red cross and ellipse show the radio position and 10% beam size ( $0.15'' \times 0.1''$ ) as position error. The cyan cross marks the possible optical counterpart. For VLA19, VLA22, VLA28, VLA36 and VLA40, the optical charts are  $1.5'' \times 1.5''$  in size given by ACS/F814W. For VLA34, the optical charts are  $3'' \times 3''$  in size given by WFC3/F814W. The red star marks the position of a known pulsar PSR J1836-2354A (M22A), and the dotted ellipse outlines the calibrated X-ray counterpart position to the pulsar given by Amato et al. (2019). The scales are also given at the lower left corner of each panel.

revealed that only one source, V2400 Oph, reaches a radio luminosity of  $\sim 10^{27}$  erg s $^{-1}$ , and notably only during an active transient state, which does not conform to VLA22. Although the X-ray and radio observations were separated by a 36 years, the 110 keV X-ray flux remained relatively stable at  $4.07 \times 10^{-14}$  erg s $^{-1}$  cm $^{-2}$  in 2005 and  $7.34 \times 10^{-14}$  erg s $^{-1}$  cm $^{-2}$  in 2014. Such low X-ray luminosities are characteristic of a quiescent state; however, since the radio data currently rely on one observation, the possibility of variability cannot be entirely excluded, needing further multi-epoch radio monitoring.

The X-ray temporal and spectral properties further support a BH nature. The lightcurve shows variability on  $\approx 10.5$  h timescales, while a Lomb-Scargle analysis yielded no periodic signals above the  $1\sigma$  confidence level—likely due to the limited observing time. Spectral modeling with a single power-law yields photon indices of  $\Gamma = 2.31_{-0.83}^{+0.95}$  and  $\Gamma = 1.06_{-0.28}^{+0.35}$  for the two epochs.

This spectral hardening at low luminosities, combined with a generally hard X-ray profile, is consistent with the advection-dominated accretion flow (ADAF) typically found in quiescent BH-LMXBs (Narayan & Yi 1995), and is notably harder than the typical spectra of quiescent NS-LMXBs which often feature a soft thermal component from the neutron star surface. Moreover, the observed spectral transition excludes a rotation-powered MSP scenario, which would maintain high spectral stability over long timescales.

Within the *Chandra* error circle, we identified two potential optical counterparts: VLA22-1 ( $M_{I_{814}} \approx 16.695 \pm 0.011$ ) and VLA22-2 ( $M_{I_{814}} \approx 21.805 \pm 0.086$ ). We extracted the  $I_{814}$  lightcurve for VLA22-1 from archival WFPC2 data. Initial fluctuations were  $< 0.1$  mag, likely dominated by instrumental noise and non-uniform CCD response rather than intrinsic variability. To mitigate these systematic effects, we performed differential photometry using an ensemble of 59 neighboring reference

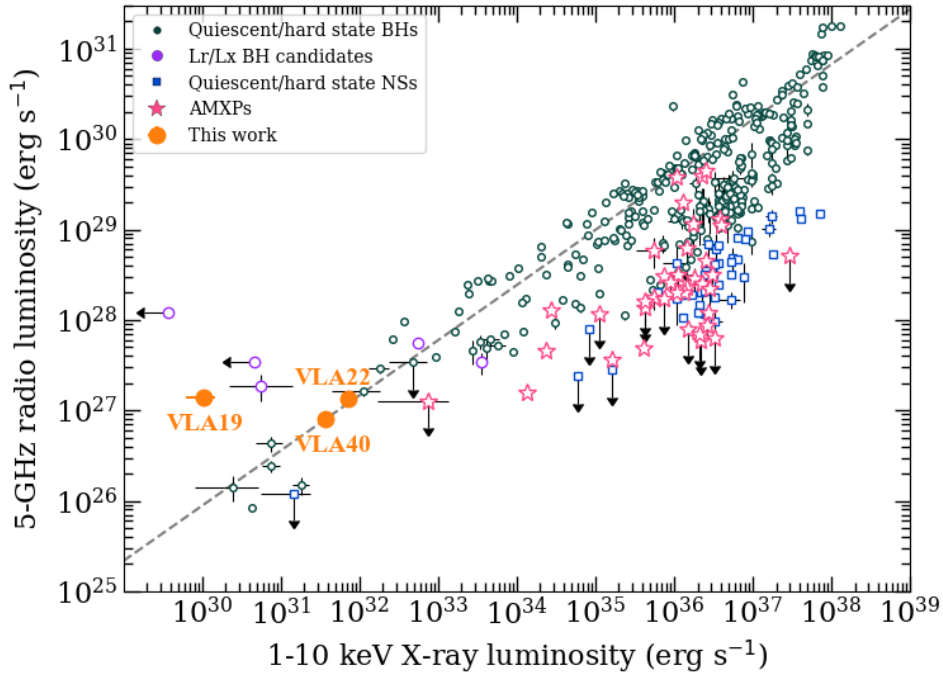


**Figure 2.** X-ray luminosity in 1-10 keV versus radio luminosity at 5 GHz of binaries. The plot and data source from the script collected by Tetarenko et al. (2016) and reference as well (Bahramian & Rushton 2022). The green circle dots are identified BH binaries and blue square dots are NS binaries in quiescence or hard state. The purple dots and blue square dots are BH candidates selected by radio observation. The pink stars are accreting millisecond X-ray pulsars (AMXPs). The grey dashed line is the  $L_R - L_X$  correlation of BH-LMXBs (Gallo et al. 2014b). The orange dots are sources we found in this work.

stars ( $16 < M_{I_{814}} < 18$ ,  $\Delta M \leq 0.1$ ). These stars exhibited systematic trends consistent with those observed in VLA22-1. After subtracting the mean ensemble variation, the calibrated lightcurve of VLA22-1 yielded a significantly reduced scatter of  $\Delta M \approx 0.04$  mag. This confirms VLA22-1 as a non-variable source within our detection limits, supporting a stable, potentially low-inclination (face-on) orbital geometry. CMD analysis (Figure 3) shows that VLA22-1 exhibits a marginal  $H\alpha$  excess, a classic tracer of an active accretion disk, while lacking the UV excess typical of CVs. By fitting its spectral energy distribution (SED) and applying extinction corrections, we estimate an effective temperature of  $T_{\text{eff}} \approx 5653 \pm 231$  K and a stellar radius of  $R_2 \approx 1.03 \pm 0.07 R_{\odot}$ . Considering that mass loss via accretion often renders donor stars undermassive compared to standard main-sequence stars of the same radius, we utilized an empirical  $M_2 - R_2$  correlation derived from confirmed BH-LMXBs to constrain the mass of VLA22-1 (Figure 4 panel (a)). The correlation,  $M_2 \propto R_2^{0.96}$ , yields an estimated donor mass of  $M_2 \approx 0.95 \pm 0.69 M_{\odot}$ . Supposing that the donor star fills its Roche-lobe, the derived radius for VLA22-1 implies an orbital period of  $P_{\text{orb}} \approx 22 \pm 8$  h (Zheng et al. 2019, Equation (3)). Narayan & McClintock (2008) demonstrated that at a given orbital period, BH systems are significantly fainter

in X-rays than NS systems due to the presence of an event horizon. As the  $L_X - P_{\text{orb}}$  plane shown in Figure 4 panel (b), VLA22-1 is more consistent with the BH region.

Alternatively, the fainter VLA22-2 ( $M_{I_{814}} \approx 21.805 \pm 0.086$ ) is also a convincing candidate for the donor star. Its redder color and position relative to the main sequence (Figure 3) suggest an evolved state, such as a faint subgiant/red giant. If VLA22-2 is indeed an evolved star, its expanded radius would imply a relatively large Roche lobe and, consequently, a long orbital period to maintain the observed low-level accretion. This scenario is physically consistent with the quiescent X-ray luminosity ( $L_X \approx 7 \times 10^{31}$  erg s $^{-1}$ ) of the system, as BH-LMXBs with evolved donors often reside in a low-accretion state for the majority of their long duty cycles (Menou et al. 1999). While both sources remain viable candidates for the true optical companion, the multi-wavelength properties—particularly the high  $L_R/L_X$  ratio and the inferred donor properties—strongly suggest that M22-VLA22 is a stellar-mass black hole undergoing low-level accretion.

### 3.2. M22-VLA19, VLA40: Potential BHs or Foreground/Background Contaminants

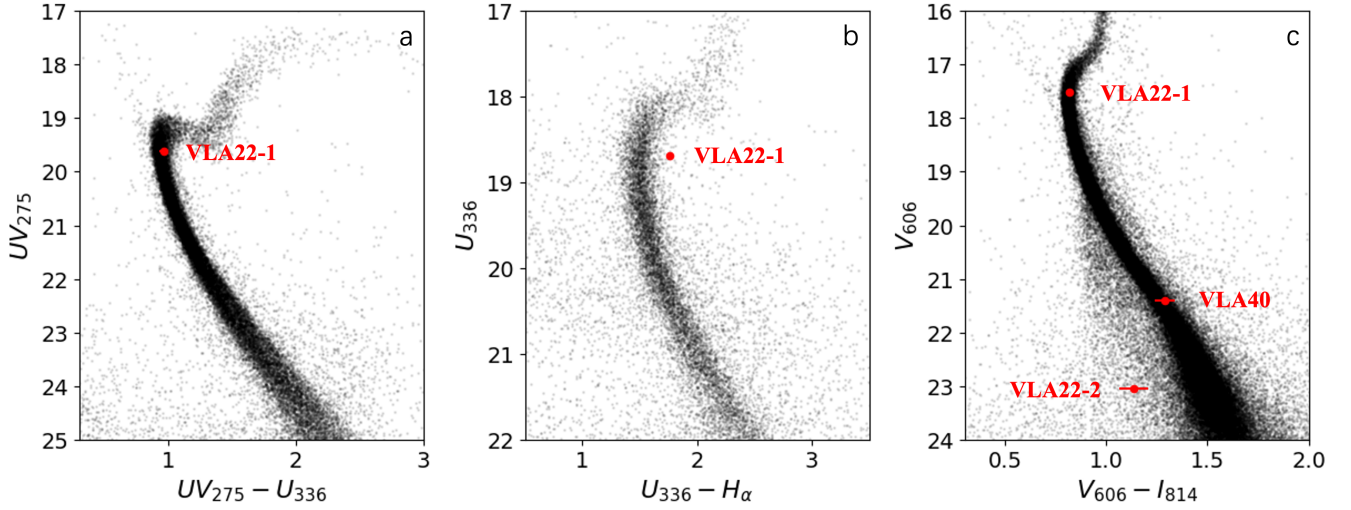


**Figure 3.** Color Map Diagram (CMD) of M22. The red dot is optical counterparts to VLA22 and VLA40, while black dots are other sources in M22. Data in panels (a) and (c) are obtained from the HUGS survey, whereas the data in panel (b) are from the HST/WFPC2 observations.

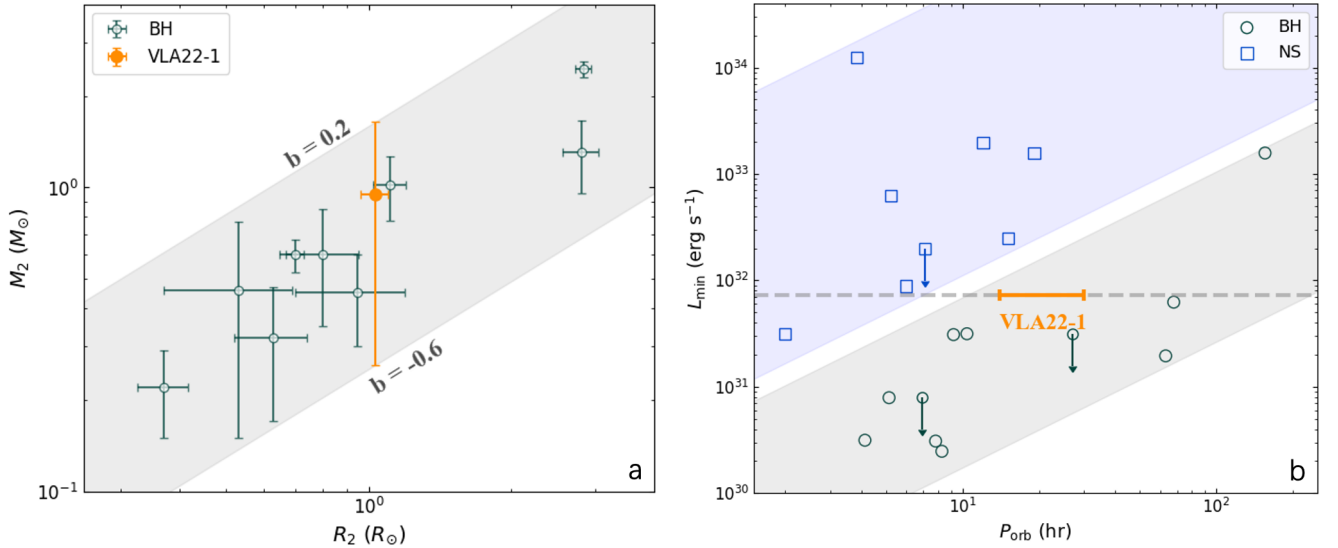


**Figure 4.** Panel (a): Mass-radius relation of donor stars in confirmed BH-LMXBs. The open green circles represent identified black hole binaries with known donor properties. The shaded region denotes the empirical parameter space defined by the relation  $\log_{10}(R_2/R_{\odot}) = 0.96 \times \log_{10}(M_2/M_{\odot}) + b$ , where the boundaries  $b = 0.2$  and  $b = -0.6$  represent the upper and lower limits of the observed distribution, respectively. The estimated  $R_2$  and  $M_2$  of VLA22-1 are also dotted in orange. Panel (b): Orbital period versus X-ray luminosity of identified binary systems regarding BH event horizon proposed by Narayan & McClintock (2008). The hollow squares represent NSs and circles are BHs. The grey line is the X-ray luminosity level of VLA22 and the orange segment represents the estimated period of VLA22-1. Reference: GRO J0422+32 (Gelino & Harrison 2003), A 0620-003 (Shahbaz et al. 1994), GRS 1009-45 (Filippenko et al. 1999), XTE J1118+480 (González Hernández et al. 2012), GRS 1124-684 (Wu et al. 2016), 4U 1543-47 (Orosz et al. 1998), XTE J1550-564 (Orosz et al. 2002), GRO J1655-40 (Orosz & Bailyn 1997), H 1705-250 (Filippenko et al. 1997), SAX J1819.3-2525 (MacDonald et al. 2014), GS 2000+251 (Ioannou et al. 2004).

VLA19 is located at a projected distance of  $2.3'$  from the cluster center, placing it between the core and the half-light radius. Its radio spectrum is highly inverted ( $\alpha = 0.79 \pm 0.39$ ), a feature strongly indicative of a self-absorbed compact jet typically associated with quiescent BH-LMXBs. The source matches a faint X-ray counterpart ( $L_X \approx 7.79 \times 10^{30} \text{ erg s}^{-1}$ ) characterized by a relatively soft spectrum ( $\Gamma = 3.28 \pm 1.44$ ). While mass segregation typically concentrates stellar-mass BHs in the cluster core, the significantly inverted radio index makes VLA19 a noteworthy candidate. Its radio properties are inconsistent with the typical steep-spectrum emission ( $\alpha \approx -0.5$ ) of background active galactic nuclei (AGNs) (Kellermann et al. 1989). If it is a cluster member, its peripheral location may suggest a history of dynamical recoil following a three-body interaction (Kulkarni et al. 1993; Sigurdsson & Hernquist 1993).

VLA40 was detected only at 5 GHz, with a  $3\sigma$  upper limit at 7 GHz ( $S_{7 \text{ GHz}} < 6.4 \pm 2.4 \mu\text{Jy}$ ) implying a spectral index of  $\alpha < 0.4$ . It is spatially coincident (offset  $\approx 0.56''$ ) with the X-ray source 2CXO J183620.4–235336, which exhibits a hard spectrum ( $\Gamma = 1.54^{+0.35}_{-0.39}$ ) typical of quiescent BHs. As shown in Figure 2, its position on the  $L_R - L_X$  plane is consistent with the BH track. A potential optical counterpart ( $M_{I_{814}} \approx 20.213 \pm 0.031$ ) was identified, showing stochastic variability of  $\sim 0.15$  mag in the WFPC2 lightcurve. This flickering could be driven by the reprocessing of fluctuating X-rays within the accretion disk or intrinsic turbulence in the accretion flow. However, we cannot rule out an extragalactic origin; the X-ray hardness and optical magnitude are also consistent with an AGN, where the observed variability would stem from stochastic disk fluctuations rather than binary interaction.

### 3.3. M22-VLA34, VLA36: Millisecond Pulsar Candidates

VLA34 is the source closest to the cluster core and is located only  $0.04''$  from 2CXO J183625.4–235451. This X-ray source has previously been associated with the 3 ms pulsar PSR J1836–2354A (M22A). After applying the optical correction from Amato et al. (2019), both VLA34 and M22A remain within the  $1\sigma$  X-ray error ellipse (Figure 1). Based on the ATNF Pulsar Catalogue, M22A has a 1.4 GHz flux density of 0.2 mJy. Extrapolating this to 5 GHz with a typical pulsar spectral index of  $\alpha = -1.6$  (Jankowski et al. 2018) yields a predicted flux of  $\approx 26 \mu\text{Jy}$ , which is marginally higher than the observed flux of VLA34. However, VLA34 is offset from the timing position of M22A by  $0.66''$ . Given the high precision of both the VLBI radio positions and the pul-

sar timing solution, a physical association between these two specific sources is unlikely.

Although VLA34 and VLA36 lack detectable optical counterparts in the crowded core region, their radio spectral indices ( $\alpha = -1.27 \pm 0.80$  and  $-2.03 \pm 0.85$ , respectively) are characteristically steep. Such values are consistent with the coherent radio emission from MSPs. The absence of optical counterparts is common for isolated rotation-powered pulsars, whose optical emission is typically well below the detection limits of current *HST* observations at GC distances. While a background AGN origin cannot be entirely excluded, their location in the crowded core and spectral steepness make them strong candidates for previously undiscovered MSPs within M22.

### 3.4. M22-VLA10, VLA25, VLA28: Likely Extragalactic Sources

VLA10 and VLA25 are located outside the *HST* field of view and both exhibit intermediate-to-steep radio spectra. VLA10 shows an exceptionally hard X-ray spectrum ( $\Gamma = 0.65^{+0.46}_{-0.60}$ ), suggesting that its soft X-ray emission is heavily suppressed by photo-electric absorption. Similarly, the best-fit absorption column for VLA25 ( $N_H = 3.54^{+3.53}_{-11.6} \times 10^{22} \text{ cm}^{-2}$ ) significantly exceeds the interstellar value of the cluster, a trait frequently observed in obscured AGNs.

VLA28 is covered by *HST* imaging but lacks a detectable optical counterpart. Its X-ray spectrum is consistent with the cluster environment ( $N_H \approx 2.82 \times 10^{21} \text{ cm}^{-2}$ ;  $\Gamma = 1.98^{+0.99}_{-1.4}$ ), but its steep radio index ( $-1.23 \pm 0.67$ ) aligns more closely with either an MSP or a background galaxy. Given that all three sources (VLA10, VLA25, and VLA28) are located at large offsets from the core where the stellar density is low, they are statistically more likely to be extragalactic background sources rather than intrinsic cluster members. We estimated the expected number of background AGNs based on the X-ray flux limits in GCcat, yielding predicted counts of 118.8, 92.8, and 72.2 within the *Chandra* position errors. These high background densities further support the likelihood that these peripheral sources are unrelated to the cluster.

## 4. CONCLUSIONS

In this study, we conducted a comprehensive multi-wavelength investigation of the globular cluster M22 by cross-matching radio observations from *VLA* with X-ray data from *Chandra* and optical photometry from *HST*. We identified eight X-ray counterparts to radio sources, six of which reside within the *HST* footprint. Our analysis suggests a diverse population of compact

objects and extragalactic contaminants, summarized as follows:

1. The BH-LMXB Candidate (VLA22): We identify VLA22 as the only radio/X-ray association in M22 whose broadband properties are consistent with a quiescent BH-LMXB. Its radio and X-ray luminosities follow the quiescent BH  $L_R - L_X$  correlation. The detected X-ray spectral hardening ( $\Gamma = 1.06_{-0.28}^{+0.35}$ ) and moderately steep radio spectrum ( $\alpha \approx -0.81 \pm 0.51$ ) are consistent with advection-dominated accretion flows. Although the lack of significant variability in the primary optical counterpart (VLA22-1) may imply a low-inclination (face-on) geometry, the inferred orbital period ( $P_{\text{orb}} \approx 22 \pm 8$  h) aligns with a BH-LMXB nature. Alternatively, the evolved red giant properties of VLA22-2 similarly necessitate a long orbital period, with both potential counterparts independently supporting a quiescent BH system. However, we note that the nominally negative radio spectral index, the non-simultaneity of the data, and the uncertain optical counterpart prevent a secure classification.
2. Potential Compact Objects (VLA19 & VLA40): VLA19 exhibits a highly inverted radio spectrum ( $\alpha = 0.79 \pm 0.39$ ), characteristic of a self-absorbed relativistic jet. Despite its location outside the core, it remains a noteworthy BH candidate, possibly representing a dynamically recoiled system. VLA40 also aligns with the BH  $L_R - L_X$  track and features a hard X-ray spectrum ( $\Gamma = 1.54_{-0.39}^{+0.35}$ ). However, its stochastic optical variability ( $\sim 0.15$  mag) and radial offset leave its classification ambiguous, as these properties are also consistent with a background AGN.
3. Millisecond Pulsar Candidates (VLA34 & VLA36): VLA34 and VLA36 are characterized by steep radio spectra ( $\alpha = -1.27 \pm 0.80$  and

$-2.03 \pm 0.85$ , respectively), indicating them as probable MSPs. Notably, our astrometric analysis suggests that VLA34 is a distinct object from the known pulsar M22A, located  $0.66''$  away. Their presence in the crowded core supports them as intrinsic cluster members and they lack optical counterparts, likely undiscovered pulsars.

4. Likely Extragalactic Sources (VLA10, VLA25, & VLA28): These sources are most likely extragalactic background objects. VLA10 and VLA25 exhibit significantly high X-ray absorption ( $N_{\text{H}}$ ) which is common in AGNs. VLA28, while possessing a radio spectrum consistent with an MSP, is located far from the cluster center, making an AGN origin statistically more probable.

Generally, the identification of M22-VLA22 as a plausible BH-LMXB consistent with recent retention models that GCs can retain stellar-mass BHs over Hubble timescales. While the nature of some sources remains elusive, our work underscores the necessity of multi-frequency diagnostics. Future high-cadence optical monitoring and VLBI proper motion studies will be essential to definitively distinguish between cluster members and background contaminants and to further constrain the BH population in M22.

*Acknowledgements* – We thank ZhiYuan Li, Yue Zhao for helpful discussion. This work was supported by the National Key R&D Program of China under grant 2023YFA1607901, the National Natural Science Foundation of China under grants 12433007 and 12221003. This research has made use of data collected by *HST*, *Chandra*, *VLA* and *ATCA*.

*Software* – CIAO, DOLPHOT, Astropy, Xspec

*Facilities:* *HST*, *Chandra*, *VLA*, *ATCA*

## REFERENCES

- Abada-Simon, M., Lecacheux, A., Bastian, T. S., Bookbinder, J. A., & Dulk, G. A. 1993, *ApJ*, 406, 692, doi: [10.1086/172479](https://doi.org/10.1086/172479)
- Amato, R., D’Ai, A., Santo, M. D., et al. 2019, *Monthly Notices of the Royal Astronomical Society*, 486, 3992, doi: [10.1093/mnras/stz1100](https://doi.org/10.1093/mnras/stz1100)
- Arnaud, K. A. 1996, in *Astronomical Society of the Pacific Conference Series*, Vol. 101, *Astronomical Data Analysis Software and Systems V*, ed. G. H. Jacoby & J. Barnes, 17
- Bahramian, A., & Rushton, A. 2022, *bersavosh/XRB-LrLx\_pub*: update 20220908, v220908, Zenodo, doi: [10.5281/zenodo.7059313](https://doi.org/10.5281/zenodo.7059313)

- Bahramian, A., Strader, J., Miller-Jones, J. C. A., et al. 2020, *The Astrophysical Journal*, 901, 57, doi: [10.3847/1538-4357/aba51d](https://doi.org/10.3847/1538-4357/aba51d)
- Brodie, J. P., & Strader, J. 2006, *ARA&A*, 44, 193, doi: [10.1146/annurev.astro.44.051905.092441](https://doi.org/10.1146/annurev.astro.44.051905.092441)
- Chomiuk, L., Strader, J., Maccarone, T. J., et al. 2013, *The Astrophysical Journal*, 777, 69, doi: [10.1088/0004-637X/777/1/69](https://doi.org/10.1088/0004-637X/777/1/69)
- Clark, G. W. 1975, *ApJL*, 199, L143, doi: [10.1086/181869](https://doi.org/10.1086/181869)
- Dolphin, A. 2016, DOLPHOT: Stellar photometry, Astrophysics Source Code Library, record ascl:1608.013. <http://ascl.net/1608.013>
- Drake, S. A., Simon, T., & Linsky, J. L. 1989, *ApJS*, 71, 905, doi: [10.1086/191402](https://doi.org/10.1086/191402)
- Evans, I. N., Primini, F. A., Glotfelty, K. J., et al. 2010, *ApJS*, 189, 37, doi: [10.1088/0067-0049/189/1/37](https://doi.org/10.1088/0067-0049/189/1/37)
- Filippenko, A. V., Leonard, D. C., Matheson, T., et al. 1999, *Publications of the Astronomical Society of the Pacific*, 111, 969, doi: [10.1086/316413](https://doi.org/10.1086/316413)
- Filippenko, A. V., Matheson, T., Leonard, D. C., Barth, A. J., & van Dyk, S. D. 1997, *Publications of the Astronomical Society of the Pacific*, 109, 461, doi: [10.1086/133902](https://doi.org/10.1086/133902)
- Fruscione, A., McDowell, J. C., Allen, G. E., et al. 2006, in *Society of Photo-Optical Instrumentation Engineers (SPIE) Conference Series*, Vol. 6270, *Observatory Operations: Strategies, Processes, and Systems*, ed. D. R. Silva & R. E. Doxsey, 62701V, doi: [10.1117/12.671760](https://doi.org/10.1117/12.671760)
- Gallo, E., Miller-Jones, J. C. A., Russell, D. M., et al. 2014a, *MNRAS*, 445, 290, doi: [10.1093/mnras/stu1599](https://doi.org/10.1093/mnras/stu1599)
- . 2014b, *MNRAS*, 445, 290, doi: [10.1093/mnras/stu1599](https://doi.org/10.1093/mnras/stu1599)
- Garmire, G. P., Bautz, M. W., Ford, P. G., Nousek, J. A., & Ricker, Jr., G. R. 2003, in *Society of Photo-Optical Instrumentation Engineers (SPIE) Conference Series*, Vol. 4851, *X-Ray and Gamma-Ray Telescopes and Instruments for Astronomy*, ed. J. E. Truemper & H. D. Tananbaum, 28–44, doi: [10.1117/12.461599](https://doi.org/10.1117/12.461599)
- Gelino, D. M., & Harrison, T. E. 2003, *The Astrophysical Journal*, 599, 1254, doi: [10.1086/379311](https://doi.org/10.1086/379311)
- González Hernández, J. I., Rebolo, R., & Casares, J. 2012, *The Astrophysical Journal*, 744, L25, doi: [10.1088/2041-8205/744/2/L25](https://doi.org/10.1088/2041-8205/744/2/L25)
- Greisen, E. W. 2003, in *Astrophysics and Space Science Library*, Vol. 285, *Information Handling in Astronomy - Historical Vistas*, ed. A. Heck, 109, doi: [10.1007/0-306-48080-8\\_7](https://doi.org/10.1007/0-306-48080-8_7)
- Harris, W. E. 1996, *AJ*, 112, 1487, doi: [10.1086/118116](https://doi.org/10.1086/118116)
- Heger, A., Fryer, C. L., Woosley, S. E., Langer, N., & Hartmann, D. H. 2003, *ApJ*, 591, 288, doi: [10.1086/375341](https://doi.org/10.1086/375341)
- Ioannou, Z., Robinson, E. L., Welsh, W. F., & Haswell, C. A. 2004, *The Astronomical Journal*, 127, 481, doi: [10.1086/380215](https://doi.org/10.1086/380215)
- Irwin, J. A., Brink, T. G., Bregman, J. N., & Roberts, T. P. 2010, *ApJL*, 712, L1, doi: [10.1088/2041-8205/712/1/L1](https://doi.org/10.1088/2041-8205/712/1/L1)
- Jankowski, F., van Straten, W., Keane, E. F., et al. 2018, *MNRAS*, 473, 4436, doi: [10.1093/mnras/stx2476](https://doi.org/10.1093/mnras/stx2476)
- Kellermann, K. I., Sramek, R., Schmidt, M., Shaffer, D. B., & Green, R. 1989, *AJ*, 98, 1195, doi: [10.1086/115207](https://doi.org/10.1086/115207)
- Krumholz, M. R., McKee, C. F., & Bland-Hawthorn, J. 2019, *ARA&A*, 57, 227, doi: [10.1146/annurev-astro-091918-104430](https://doi.org/10.1146/annurev-astro-091918-104430)
- Kulkarni, S. R., Hut, P., & McMillan, S. 1993, *Nature*, 364, 421, doi: [10.1038/364421a0](https://doi.org/10.1038/364421a0)
- MacDonald, R. K. D., Bailyn, C. D., Buxton, M., et al. 2014, *The Astrophysical Journal*, 784, 2, doi: [10.1088/0004-637X/784/1/2](https://doi.org/10.1088/0004-637X/784/1/2)
- Marsh, T. R., Gänsicke, B. T., Hümmerich, S., et al. 2016, *Nature*, 537, 374, doi: [10.1038/nature18620](https://doi.org/10.1038/nature18620)
- McMullin, J. P., Waters, B., Schiebel, D., Young, W., & Golap, K. 2007, in *Astronomical Society of the Pacific Conference Series*, Vol. 376, *Astronomical Data Analysis Software and Systems XVI*, ed. R. A. Shaw, F. Hill, & D. J. Bell, 127
- Menou, K., Esin, A. A., Narayan, R., et al. 1999, *ApJ*, 520, 276, doi: [10.1086/307443](https://doi.org/10.1086/307443)
- Miller-Jones, J. C. A., Strader, J., Heinke, C. O., et al. 2015, *Monthly Notices of the Royal Astronomical Society*, 453, 3919, doi: [10.1093/mnras/stv1869](https://doi.org/10.1093/mnras/stv1869)
- Morscher, M., Umbreit, S., Farr, W. M., & Rasio, F. A. 2013, *ApJL*, 763, L15, doi: [10.1088/2041-8205/763/1/L15](https://doi.org/10.1088/2041-8205/763/1/L15)
- Narayan, R., & McClintock, J. E. 2008, *New Astronomy Reviews*, 51, 733, doi: [10.1016/j.newar.2008.03.002](https://doi.org/10.1016/j.newar.2008.03.002)
- Narayan, R., & Yi, I. 1995, *ApJ*, 452, 710, doi: [10.1086/176343](https://doi.org/10.1086/176343)
- Nardiello, D., Libralato, M., Piotto, G., et al. 2018, *MNRAS*, 481, 3382, doi: [10.1093/mnras/sty2515](https://doi.org/10.1093/mnras/sty2515)
- Orosz, J. A., & Bailyn, C. D. 1997, *The Astrophysical Journal*, 477, 876, doi: [10.1086/303741](https://doi.org/10.1086/303741)
- Orosz, J. A., Jain, R. K., Bailyn, C. D., McClintock, J. E., & Remillard, R. A. 1998, *The Astrophysical Journal*, 499, 375, doi: [10.1086/305620](https://doi.org/10.1086/305620)
- Orosz, J. A., Groot, P. J., van der Klis, M., et al. 2002, *The Astrophysical Journal*, 568, 845, doi: [10.1086/338984](https://doi.org/10.1086/338984)
- Osten, R. A., Brown, A., Ayres, T. R., et al. 2000, *ApJ*, 544, 953, doi: [10.1086/317249](https://doi.org/10.1086/317249)
- Piotto, G., Milone, A. P., Bedin, L. R., et al. 2015, *AJ*, 149, 91, doi: [10.1088/0004-6256/149/3/91](https://doi.org/10.1088/0004-6256/149/3/91)

- Ridder, M. E., Heinke, C. O., Sivakoff, G. R., & Hughes, A. K. 2023, MNRAS, 519, 5922, doi: [10.1093/mnras/stad038](https://doi.org/10.1093/mnras/stad038)
- Russell, T. D., Miller-Jones, J. C. A., Sivakoff, G. R., et al. 2016, MNRAS, 460, 3720, doi: [10.1093/mnras/stw1238](https://doi.org/10.1093/mnras/stw1238)
- Shahbaz, T., Naylor, T., & Charles, P. A. 1994, Monthly Notices of the Royal Astronomical Society, 268, 756, doi: [10.1093/mnras/268.3.756](https://doi.org/10.1093/mnras/268.3.756)
- Shishkovsky, L., Strader, J., Chomiuk, L., et al. 2018, The Astrophysical Journal, 855, 55, doi: [10.3847/1538-4357/aaadb1](https://doi.org/10.3847/1538-4357/aaadb1)
- . 2020, The Astrophysical Journal, 903, 73, doi: [10.3847/1538-4357/abb880](https://doi.org/10.3847/1538-4357/abb880)
- Sigurdsson, S., & Hernquist, L. 1993, Nature, 364, 423, doi: [10.1038/364423a0](https://doi.org/10.1038/364423a0)
- Sippel, A. C., & Hurley, J. R. 2013, MNRAS, 430, L30, doi: [10.1093/mnrasl/sls044](https://doi.org/10.1093/mnrasl/sls044)
- Sirianni, M., Jee, M. J., Benítez, N., et al. 2005, PASP, 117, 1049, doi: [10.1086/444553](https://doi.org/10.1086/444553)
- Strader, J., Chomiuk, L., Maccarone, T. J., Miller-Jones, J. C. A., & Seth, A. C. 2012, Nature, 490, 71, doi: [10.1038/nature11490](https://doi.org/10.1038/nature11490)
- Tetarenko, B. E., Bahramian, A., Arnason, R. M., et al. 2016, ApJ, 825, 10, doi: [10.3847/0004-637X/825/1/10](https://doi.org/10.3847/0004-637X/825/1/10)
- Tudor, V., Miller-Jones, J. C. A., Strader, J., et al. 2022, Monthly Notices of the Royal Astronomical Society, 513, 3818, doi: [10.1093/mnras/stac1034](https://doi.org/10.1093/mnras/stac1034)
- Webb, N., & Servillat, M. 2013, Astronomy & Astrophysics, 551, A60, doi: [10.1051/0004-6361/201117229](https://doi.org/10.1051/0004-6361/201117229)
- Webb, N. A., Serre, D., Gendre, B., et al. 2004, Astronomy & Astrophysics, 424, 133, doi: [10.1051/0004-6361:20040399](https://doi.org/10.1051/0004-6361:20040399)
- Wu, J., Orosz, J. A., McClintock, J. E., et al. 2016, The Astrophysical Journal, 825, 46, doi: [10.3847/0004-637X/825/1/46](https://doi.org/10.3847/0004-637X/825/1/46)
- Zheng, L.-L., Gu, W.-M., Yi, T., et al. 2019, AJ, 158, 179, doi: [10.3847/1538-3881/ab449f](https://doi.org/10.3847/1538-3881/ab449f)